

All-graphene integrated circuits via strain engineering

Vitor M. Pereira and A. H. Castro Neto

Department of Physics, Boston University,

590 Commonwealth Avenue, Boston, MA 02215, USA

(Dated: February 20, 2024)

Abstract

We propose a route to all-graphene integrated electronic devices by exploring the influence of strain on the electronic structure of graphene. We show that strain can be easily tailored to generate electron beam collimation, 1D channels, surface states and confinement, the basic elements for all-graphene electronics. In addition this proposal has the advantage that patterning can be made on substrates rather than on the graphene sheet, thereby protecting the integrity of the latter.

PACS numbers: 81.05.Uw, 85.30.Mn, 73.90.+f

Notwithstanding its atomic thickness, graphene sheets have been shown to accommodate a wealth of remarkable fundamental properties, and to hold sound prospects in the context of a new generation of electronic devices and circuitry [1]. The exciting prospect about graphene is that, not only can we have extremely good conductors, but also most active devices made out of graphene. One of the current difficulties with respect to this lies in that conventional electronic operations require the ability to completely pinch-off the charge transport on demand. Although the electric field effect is impressive in graphene [2], the existence of a minimum of conductivity poses a serious obstacle towards desirable on/off ratios. A gapped spectrum would certainly be instrumental. The presence of a gap is implicitly related to the problem of electron confinement, which for Dirac fermions is not easily achievable by conventional means (like electrostatic potential wells) [3]. Geometrical confinement has been achieved in graphene ribbons and dots [4, 5], but the sensitivity of transport to the edge profile [6], and the inherent difficulty in the fabrication of such microstructures with sharply defined edges remains a problem.

The ultimate goal would be an all-graphene circuit. This could be achieved by taking a graphene sheet and patterning the different devices and leads by means of appropriate cuts that would generate leads ribbons, dots, etc.. This *papercutting* electronics can have serious limitations with respect to reliability, scalability, and is prone to damaging and inducing disorder in the graphene sheet [7]. Therefore, in keeping with the paper art analogy, we propose an alternative *origami* electronics [8].

We show here that all the characteristics of graphene ribbons and dots (viz. geometrical quantization, 1D channels, surface modes) might be locally obtained by patterning, *not graphene*, but the substrate on which it rests. The essential aspect of our approach is the generation of strain in the graphene lattice capable of changing the in-plane hopping amplitude in an anisotropic way. This can be achieved by means of appropriate geometrical patterns in an homogeneous substrate (grooves, creases, steps or wells), or by means of an heterogeneous substrate in which different regions interact differently with the graphene sheet, generating different strain profiles [Fig. 1(b)]. Another design alternative consists in depositing graphene onto substrates with regions that can be controllably strained on demand [9]. Through a combination of folding and/or clamping a graphene sheet onto such substrate patterns, one might generate local strain profiles suitable for the applications discussed in detail below, while preserving a whole graphene sheet.

The remainder of the paper is dedicated to show how strain only can be used as a means of achieving: (i) direction dependent tunneling (ii) beam collimation, (iii) confinement, (iv) the spectrum of an effective ribbon, (v) 1D channels, and (vi) surface modes.

Model – Within a tight-binding formulation of the electronic motion [10], effects of in-plane strain can be captured, to leading order, by considering the changes in nearest-neighbor hopping amplitude, t . We write $t(\mathbf{R}_i, \mathbf{n}) = t + \delta t(\mathbf{R}_i, \mathbf{n})$, and treat the space dependent strain-induced modulation, δt , as a perturbation ($t \approx 3\text{ eV}$). It is straightforward to show [10] that, for smooth perturbations, the low energy Hamiltonian is

$$H = v_F \int d\mathbf{r} \Psi^\dagger \begin{bmatrix} \boldsymbol{\sigma} \cdot (\mathbf{p} - \frac{1}{v_F} \mathcal{A}) & 0 \\ 0 & -\boldsymbol{\sigma} \cdot (\mathbf{p} + \frac{1}{v_F} \mathcal{A}) \end{bmatrix} \Psi, \quad (1)$$

valid near the valleys K and K' in the Brillouin zone, with $\boldsymbol{\sigma} = (\sigma_x, \sigma_y, \sigma_z)$, $v_F = 3ta/2\hbar$ and $\Psi = [\psi_K^A(\mathbf{r}), \psi_K^B(\mathbf{r}), \psi_{K'}^B(\mathbf{r}), \psi_{K'}^A(\mathbf{r})]^\dagger$ is a spinor containing the electron fields in each sublattice and valley. Within each valley it has the form $H = v_F \boldsymbol{\sigma} \cdot (\mathbf{p} - \frac{1}{v_F} \mathcal{A})$, so that electron dynamics is determined by a Dirac equation in the presence of a gauge field \mathcal{A} . This field stems from the perturbation to the homogeneous hopping amplitudes and is related to $\delta t(\mathbf{R}, \mathbf{n})$ via the complex vector potential (VP) $\mathcal{A}(\mathbf{r}) = \mathcal{A}_x(\mathbf{r}) - i\mathcal{A}_y(\mathbf{r})$:

$$\mathcal{A}(\mathbf{r}) = \sum_{\mathbf{n}} \delta t(\mathbf{r}, \mathbf{n}) e^{i\mathbf{K} \cdot \mathbf{n}} \quad (2)$$

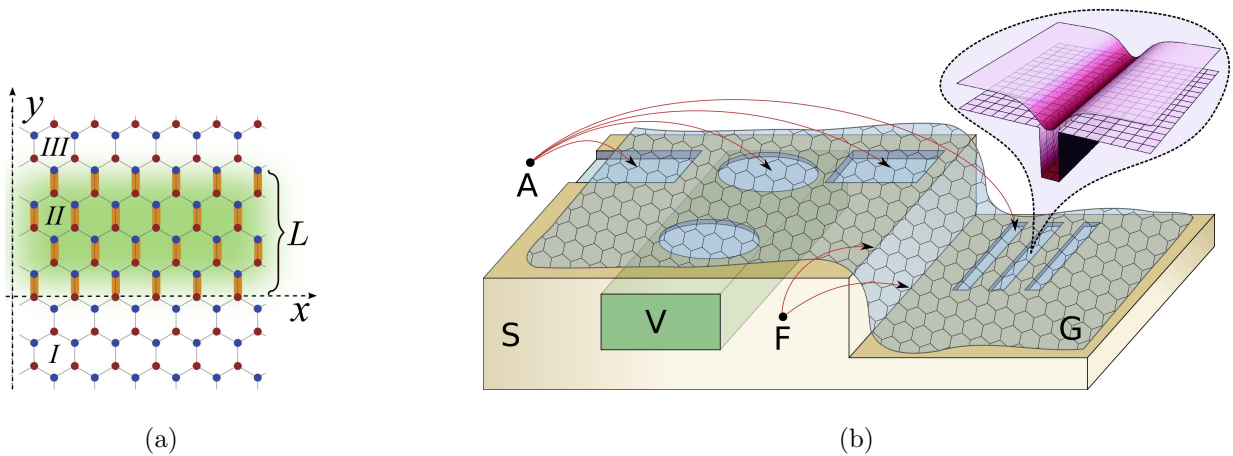


FIG. 1: (Color online) (a) Lattice orientation considered in the text. Thicker bonds have perturbed hopping. (b) Artistic depiction of a substrate (S) patterned with folds (F), trenches, dots and wells (A), upon which rests a graphene sheet (G).

The fact that \mathcal{A} appears in (1) with its sign reversed for the K' valley guarantees overall time reversal symmetry. For definiteness, with the lattice orientation shown in Fig. 1(a) we perturb the vertical hopping by a constant amount δt , over a finite region of width L . The perturbation and the associated $\mathcal{A}(\mathbf{r})$ are

$$\delta t(\mathbf{R}_i, \mathbf{n}) = \delta t \delta_{\mathbf{n},0} \theta(Y_i) \theta(L - Y_i) \quad (3a)$$

$$\mathcal{A}(\mathbf{r}) = \delta t \theta(y) \theta(L - y) \mathbf{u}_x. \quad (3b)$$

The gauge field \mathcal{A} is oriented along \mathbf{u}_x , which coincides with the direction of translational invariance. Using units where $v_F = \hbar = 1$, and allowing for the presence of an electrostatic potential $V(\mathbf{r})$ in the barrier region, the wave equations for the K valley can then be cast as

$$[-i\partial_x - \partial_y - \mathcal{A}_x(y)] \psi^B(\mathbf{r}) = [E - V(\mathbf{r})] \psi^A(\mathbf{r}) \quad (4a)$$

$$[-i\partial_x + \partial_y - \mathcal{A}_x(y)] \psi^A(\mathbf{r}) = [E - V(\mathbf{r})] \psi^B(\mathbf{r}). \quad (4b)$$

In this formulation, the problem reduces to the study of Dirac electrons in the presence of VP and electrostatic barriers, and is related to corresponding studies of Dirac electrons in the presence of magnetic barriers [11, 12, 13, 14]. The profile (3b) has also been considered in Ref. 15 in modelling a suspended graphene sheet.

Tunneling – We begin by analyzing the tunneling characteristics across the barrier-like perturbation of Eq. (3). Without compromising generality [16], in the remainder of the paper we shall be concerned with the situation $\delta t > 0$ and $E > 0$. We parametrize the wavefunction in the three regions of Fig. 1(a) as

$$\begin{aligned} \Psi^I &= e^{ik_x x + ik_y y} \begin{pmatrix} 1 \\ e^{i\phi} \end{pmatrix} + R e^{ik_x x - ik_y y} \begin{pmatrix} 1 \\ e^{-i\phi} \end{pmatrix} \\ \Psi^{II} &= C_1 \begin{pmatrix} 1 \\ e^{i\varphi} \end{pmatrix} e^{ik_x x + iq_y y} + C_2 \begin{pmatrix} 1 \\ e^{-i\varphi} \end{pmatrix} e^{ik_x x - iq_y y} \\ \Psi^{III} &= T e^{ik_x x + ik_y y} \begin{pmatrix} 1 \\ e^{i\phi} \end{pmatrix} \end{aligned}$$

where we have the kinetic momenta $k_x = E \cos \phi$, $k_x - \delta t = E \cos \varphi$, $q_y = E \sin \varphi$ and the energy $E^2 = k_x^2 + k_y^2 = (k_x - \delta t)^2 + q_y^2$. Substitution in the wave equation (4) leads to the following transmission amplitude [13, 15]:

$$T = \frac{e^{-ik_y L} \sin \phi \sin \varphi}{\cos(q_y L) \sin \phi \sin \varphi + i \sin(q_y L) (\cos \phi \cos \varphi - 1)}. \quad (5)$$

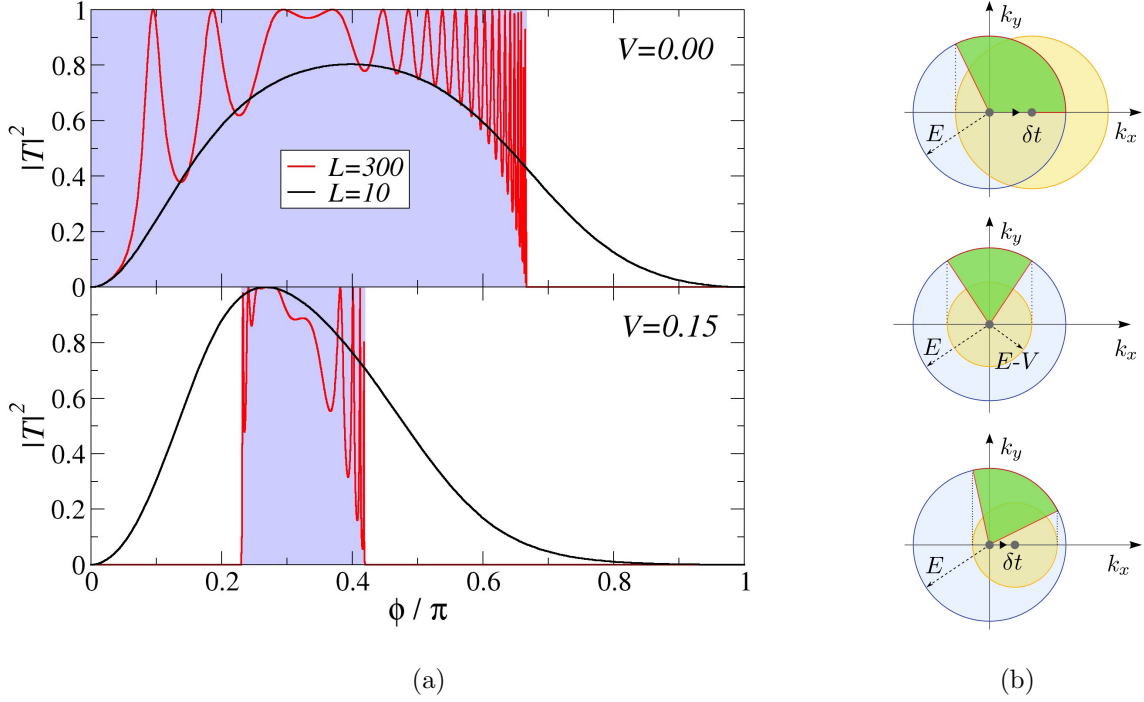


FIG. 2: (Color online) Transmission obtained from (5) for $L = 10, 300$, $\delta t = 0.1$, $E = 0.2$ with (bottom) and without (top) gate potential V . On the right we depict the phase space for the cases where only the strain induced VP is present ($\mathcal{A}_x \neq 0$, $V = 0$), for a pure gate potential ($\mathcal{A}_x = 0$, $V \neq 0$) and for a combination of both ($\mathcal{A}_x \neq 0$, $V \neq 0$). The shaded (green) sectors represent the range of incident angles ϕ which are not filtered by the barrier.

This result is valid also for $V \neq 0$ with the appropriate substitution $E \rightarrow E - V$ inside the barrier. As pointed out in the case of a real magnetic field [17], conservation of k_x requires $E \cos \phi = \delta t + E \cos \varphi$, leading to strong suppression of tunneling for $\phi > \arccos(-1 + \delta t/E)$. When such condition is in effect, the internal angle has to be analytically continued to the imaginary axis $\varphi \rightarrow i\varphi$, $q_y \rightarrow iq_y$ causing an exponential suppression of $|T|^2$. Moreover, if $\delta t/E > 2$ tunneling is completely suppressed. These effects are illustrated in Fig. 2(a) where we plot $|T|^2$ for different values of L and V .

Beam Collimation – Several aspects can be immediately identified from Fig. 2. Klein tunneling [3] is absent for a pure VP barrier, and if $V \neq 0$ Klein tunneling might persist albeit at $\phi \neq \pi/2$. As hinted above, for wide barriers tunneling is highly suppressed for certain ranges of ϕ that depend on δt , E and V . This filtering effect for certain incidence angles is best appreciated by inspecting the phase space pictures shown in Fig. 2(b): the effect of \mathcal{A}_x

is to translate the Fermi surface $E^2 = k_x^2 + k_y^2$ by δt along the horizontal axis. Conservation of energy and momentum immediately leads to a sector of allowed incident angles, as drawn. Analogous reasoning applies for a pure electrostatic barrier (where the Fermi surface in the barrier changes size) or a combination of both. In all cases this geometrical construction immediately yields the transmission sector. It is clear that, whereas in a purely electrostatic barrier the transmission sector is symmetric with respect to normal incidence ($\phi = \pi/2$), in a VP barrier this sector always contains either $\phi = 0$ or π , depending on the relative sign of E and δt . Combining these two cases one can generate virtually any transmission sector with a single barrier, as exemplified in Fig. 2.

This has immediate applicability in electron beam collimation and lensing, and the effect is easily amplifiable through a series of barriers [13]. In addition, the beam refracted by the barrier can approach or recede from the normal interchangeably by changing the sign of δt . Alternatively, since the transmission sector depends explicitly on E , a suitable geometrical configuration of barriers can be used to filter the energy of the incoming beam. In addition, the suppression of tunnelling for certain angular sectors leads to the appearance of a transport gap, as shown in Ref. 15. Therefore, even though small strain does not lead to a bulk spectral gap, the system exhibits an effective transport gap. Within the allowed sector, transmission through wider barriers is additionally characterized by a series of marked resonances where $|T|^2 = 1$, and electron flow is totally unhindered. Such behavior, usually associated with successive internal reflections, strongly suggests the possibility of confinement.

Confinement – Dirac electrons are notoriously resilient to conventional confinement strategies on account of the Klein paradox [3]. The fact that our VP barriers exponentially suppress electronic transmission will be further explored to confine Dirac electrons. A confined state inside the barrier has the form

$$\begin{aligned}\Psi^I &= A e^{ik_x x} e^{\kappa y} \begin{pmatrix} 1 \\ e^{\vartheta} \end{pmatrix}, \quad \Psi^{III} = D e^{ik_x x} e^{-\kappa y} \begin{pmatrix} 1 \\ e^{-\vartheta} \end{pmatrix}, \\ \Psi^{II} &= B e^{ik_x x} e^{ik_y y} \begin{pmatrix} 1 \\ e^{i\varphi} \end{pmatrix} + C e^{ik_x x} e^{-ik_y y} \begin{pmatrix} 1 \\ e^{-i\varphi} \end{pmatrix}.\end{aligned}\tag{6}$$

From the wave equation it follows that $E^2 = k_x^2 - \kappa^2 = (k_x - \delta t)^2 + k_y^2$, $k_x = E \cosh \vartheta$, $\kappa = E \sinh \vartheta$, $k_x - \delta t = E \cos \varphi$, $k_y = E \sin \varphi$. From the fact that $E^2 > 0$, this type of solution requires $|k_x - \delta t| < |E| < |k_x|$. This is graphically represented by region 2 in

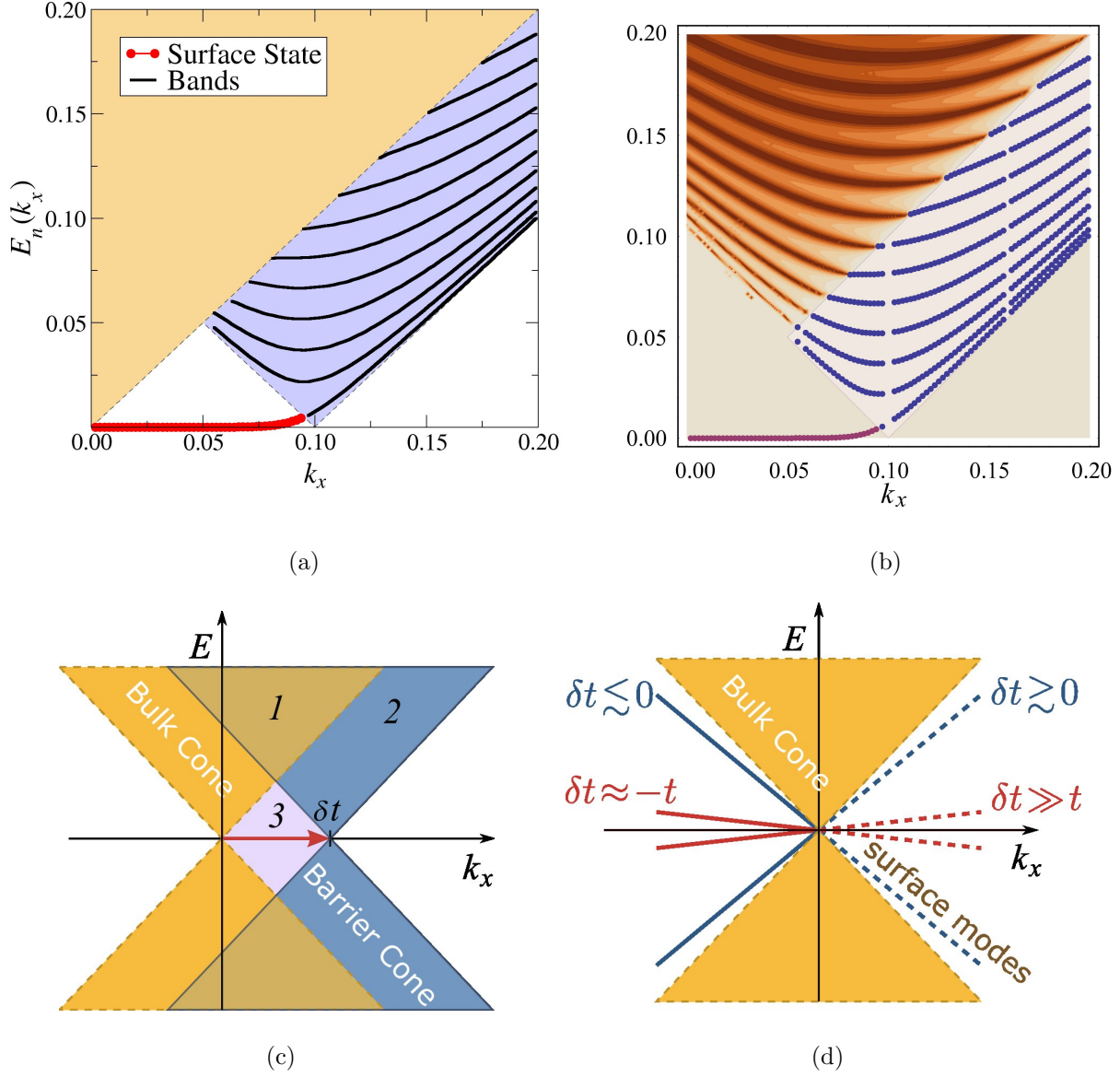


FIG. 3: (Color online) (a) Dispersion of the confined solutions, $E_n(k_x)$ for $\delta t = 0.1$ and $L = 200$. (b) A density plot of the transmission $t(E, k_x)$ from Eq. (5) is shown in the upper region (region 1), which is plotted together with the same data as in panel (a). (c) Regions 1, 2 and 3 discussed in the text. (d) Linearly dispersing modes for the narrow barrier discussed in the text.

Fig. 3(c). In addition, continuity of the wavefunction requires that

$$\cot(k_y L) \sin \varphi \sinh \vartheta = 1 - \cos \varphi \cosh \vartheta \quad (7)$$

be satisfied. When solved for E , Eq. (7) yields a discrete spectrum of energies for each value

of k_x : $E_n(k_x)$. Region 2 shown in Fig. 3(c) is therefore characterized by the emergence of *1D channels (quantum wire) confined to the barrier region*, and dispersing along k_x . A particular realization of this effect is shown in Fig. 3(a). It is clear from this figure and Eqs. (6,7) that such states share all the features of the 1D modes typical of graphene nanoribbons. In particular, at the displaced Dirac point the spectrum scales as $E_n(k_x = \delta t) \approx (n + 1/2)\pi/L$ and, for all purposes related to the electronic states and spectrum, in region 2 this system behaves as a nanoribbon. This includes the energy scales associated with the confinement gaps. For example, the gap is roughly $E_g \approx 1/L$ eV.nm, so that $L \approx 20$ nm yields a gap of ≈ 50 meV. This is valid as long as $\delta t \gg E_g$, which should be the case for $\delta t/t \sim 10\%$. Hopping variations of this magnitude can be achieved with a local strain of $\sim 5\%$ [18].

Surface Modes – The similarity of a VP barrier with the physics of a nanoribbon achieves its fullest if one notices that surface states are also possible. Just like the edge modes of zig-zag nanoribbons, we consider a state localized at the barrier edges. Such state should decay to both sides of $y = 0$ and $y = L$ simultaneously. Consequently we can construct its wavefunction from Eq. (6) through analytical continuation of k_y to the imaginary axis: $k_x \rightarrow i\kappa'$. The energy will be $E^2 = k_x^2 - \kappa^2 = (k_x - \delta t)^2 - \kappa'^2$, which restricts the space of solutions to the areas outside both Dirac cones [Fig. 3(c)]. The solution for the wavefunction so constructed leads to a quantization condition analogous to (7) but, since the circular functions are converted to hyperbolic, will admit only one solution, valid precisely when $0 < k_x \leq \delta t$ [region 3 of Fig. 3(c)]. In region 3 we then have a single state, whose dispersion is shown in Fig. 3(a). This mode smoothly merges with the lowest state in region 2 and, in the limit of $L \rightarrow \infty$ its energy is given by $E \approx 2(\delta t - k_x)\sqrt{\frac{k_x}{\delta t}} e^{-L(\delta t - k_x)}$, making clear that this mode's energy decays exponentially from the shifted Dirac point towards $k_x = 0$. Inspection of the solution in this limit reveals that the amplitude in one sublattice becomes much smaller than in the other, in complete analogy to the edge states in a wide nanoribbon. It is straightforward to demonstrate that such surface states persist in the limit $L = \infty$ where the problem reduces to a VP step. For a step, the surface modes have strictly zero energy, and occupy only one sublattice [19].

The results shown in Fig. 3(a) are symmetric with respect to $E = 0$ [16]. This figure shows that the region $2 \cup 3$, lying outside the continuum of the bulk of the system, supports spatially confined 1D modes, which have the same characteristics as modes in a ribbon, including the presence of surface states. We can now coherently interpret what happens in region 1,

in connection with the tunneling calculations described earlier: just as in a conventional Schrödinger-like barrier, the scattering states in region 1 (the bulk continuum) should “feel” the presence of the confined solutions inside the barrier. This manifests itself through the transmission resonances already shown in Fig. 2(a). In fact, when the transmission (5) is plotted in the (E, k_x) plane, we obtain the result shown in region 1 of Fig. 3(b). The darker regions of this density plot correspond to the transmission resonances, which lie in the extrapolation of the confined modes into the bulk continuum.

Narrow Limit – The approach used so far begs revision for the case of very narrow and/or large perturbations in the hopping. The clearest example is the case where L approaches the lattice spacing, so that hopping is perturbed only in one unit cell along \mathbf{u}_y . Clearly, if $\delta t = -t$ the upper and lower half planes become disconnected and no tunneling is expected. This, however, is not captured by Eq. (5) which assumes overall continuity of the wavefunction and small perturbations. Since the narrow limit is of interest, e.g. in the case of a tight graphene crease, we tackle it by analyzing the localized perturbation

$$\delta t(\mathbf{R}_i, \mathbf{n}) = \delta t \delta_{\mathbf{n},0} \delta_{Y_i,0} \Rightarrow \mathcal{A}(\mathbf{r}) = \hbar v_F \frac{\delta t}{t} \delta(y) \mathbf{u}_x. \quad (8)$$

One consequence of the first order nature of the Dirac equation (4) is the discontinuity of the wavefunction in the presence of this potential. The presence of $\delta(y)$ in (8) imposes a boundary condition at the origin. In our case, there is the peculiarity that the weight of $\delta(y)$ cannot be even for both sublattices: for the geometry of Fig. 1(a) the appropriate integration of this Dirac-delta is

$$\int_{0^-}^{0^+} dy \psi^{A,B}(x, y) \delta(y) = \psi^{A,B}(x, 0^{+,-}) \quad (9)$$

leading to the boundary conditions $\psi^B(0^-) = \eta \psi^B(0^+)$ and $\psi^A(0^+) = \eta \psi^A(0^-)$, with $\eta = 1 + \delta t/t$. The wavefunction is naturally discontinuous and, moreover, for $\delta t = -t$ ($\eta = 0$) vanishes in different sublattices at the upper and lower half-plane. Notice that in the case $\delta t = -t$ the system is comprised of two independent semi-planes with a zig-zag termination. Our BC reproduces the correct BC for these two zig-zag semi-planes [10, 20]. The transmission and reflection amplitudes as a function of $\phi = \arg(k_x + ik_i)$ read

$$R = \frac{1 - \eta^2}{\eta^2 - e^{-2i\phi}}, \quad T = \eta \frac{1 - e^{-2i\phi}}{\eta^2 - e^{-2i\phi}}, \quad (10)$$

with $|R|^2 + |T|^2 = 1$, and $T = 0$ for $\eta = 0$ as expected. The interesting fact about such narrow barriers is that *they still support surface modes*. Applying the same procedure outlined above

to the case (8) one straightforwardly obtains a state that decays exponentially to both sides of the axis $y = 0$. Its dispersion is given by $E(k_x) = \pm v_s |k_x|$ where $v_s = 2|\eta|/(1+\eta^2)$ and such states exist for $k_x > 0$ ($k_x < 0$) when $\eta^2 > 1$ ($\eta^2 < 1$). This is a very interesting situation: the perturbation of a single row of hoppings leads to the emergence of linearly-dispersing 1D modes that live along the perturbed line. These modes detach from the continuum for small δt ($E \lesssim \pm |k_x|$), and reach zero energy at $\delta t = -t$, just as expected for the two zig-zag semiplanes that result in that limit. This effect is illustrated in Fig. 3(d).

In summary, our approach demonstrates that strain-induced gauge fields can be tailored to generate confined states, quantum wires and collimation in graphene. These results, together with the fact that strain has been reliably controlled in graphene [9], opens an exciting prospect towards all-graphene electronics.

We acknowledge the hospitality of the Aspen Center for Physics, where this work germinated. VMP is supported by FCT via SFRH/BPD/27182/2006 and PTDC/FIS/64404/2006. AHCN was partially supported by the U.S. DOE under the grant DE-FG02-08ER46512.

-
- [1] A. K. Geim and K. S. Novoselov, Nat. Mat. **6**, 183 (2007).
 - [2] K. S. Novoselov *et al.*, Science **306**, 666 (2004).
 - [3] M. I. Katsnelson, K. S. Novoselov, and A. K. Geim, Nat. Phys. **2**, 620 (2006).
 - [4] M. Y. Han *et al.*, Phys. Rev. Lett. **98**, 206805 (2007).
 - [5] L. A. Ponomarenko *et al.*, Science **320**, 356 (2008).
 - [6] E. R. Mucciolo, A. H. Castro Neto, and C. H. Lewenkopf, Phys. Rev. B **79**, 075407 (2009).
 - [7] F. Sols, F. Guinea, and A. H. Castro Neto, Phys. Rev. Lett. **99**, 166803 (2007).
 - [8] D. Tománek, Physica B: Cond. Mat. **323**, 86 (2002).
 - [9] Z. H. Ni *et al.*, arXiv:0810.3476 (2008).
 - [10] A. H. Castro Neto *et al.*, Rev. Mod. Phys. **81**, 109 (2009).
 - [11] H. Xu, T. Heinzl, M. Evaldsson, and I. V. Zozoulenko, Phys. Rev. B **77**, 245401 (2008).
 - [12] M. R. Masir *et al.*, Phys. Rev. B **77**, 235443 (2008).
 - [13] S. Ghosh and M. Sharma, arXiv:0806.2951 (2008).
 - [14] L. Dell'Anna and A. D. Martino, Phys. Rev. B **79**, 045420 (2009).

- [15] M. M. Fogler, F. Guinea, and M. I. Katsnelson, Phys. Rev. Lett. **101**, 226804 (2008).
- [16] Our results are symmetric with respect to $E \rightarrow -E$. When $\delta t \rightarrow -\delta t$ the Dirac cone is shifted in the opposite direction and thus our results should be reflected along the axis $k_x = 0$.
- [17] A. D. Martino, L. Dell'Anna, and R. Egger, Phys. Rev. Lett. **98**, 066802 (2007).
- [18] V. M. Pereira, A. H. Castro Neto, and N. M. R. Peres, arXiv:0811.4396 (2008).
- [19] The sign of δt in the step determines which sublattice.
- [20] For the orientation of Fig. 1(a) there are no intervalley terms, just as in the case of a pure zig-zag edge.